European Journal of Medicinal Chemistry 213 (2021) 113184

Contents lists available at ScienceDirect

European Journal of Medicinal Chemistry

journal homepage: http://www.elsevier.com/locate/ejmech

Research paper

Effect of structural variation on tumor targeting efficacy of cationically charged porphyrin derivatives: Comparative *in-vitro* and *in-vivo evaluation* for possible potential in PET and PDT

Mohini Guleria [a], Shishu K. Suman [a], Jyotsna B. Mitra [a], Sandeep B. Shelar [b], Jeyachitra Amirdhanayagam [a], Haladhar D. Sarma [c], Ashutosh Dash [a, d], Tapas Das [a, d, *]

[a] Radiopharmaceuticals Division, Bhabha Atomic Research Centre, Trombay, Mumbai, 400085, India
[b] Chemistry Division, Bhabha Atomic Research Centre, Trombay, Mumbai, 400085, India
[c] Radiation Biology and Health Sciences Division, Bhabha Atomic Research Centre, Trombay, Mumbai, 400085, India
[d] Homi Bhabha National Institute, Anushaktinagar, Mumbai, 400094, India

ARTICLE INFO

Article history:
Received 28 May 2020
Received in revised form
7 January 2021
Accepted 7 January 2021
Available online 16 January 2021

Keywords:
Cationic porphyrin
Radiolabeled porphyrin
Photocytotoxicity
PET

ABSTRACT

Tetracationic (TMPyP) and tricationic porphyrin (TriMPyCOOHP) derivatives were synthesized, characterized and investigated for binding with DNA by Isothermal Titration Calorimetry as well as by UV–Vis spectroscopy in order to study the effect of structural variation on tumor targeting efficacy of cationically charged porphyrin derivatives. Fluorescence cell imaging studies performed in cancer cell lines corroborated the findings of aforementioned studies. Photocytotoxicity experiments in A549 cell lines revealed relatively higher light dependent cytotoxic effects exerted by TMPyP compared to TriMPyCOOHP. *In-vivo* experiments in tumor bearing animal model revealed relatively longer retention of ^{68}Ga-TMPyP in tumorous lesion compared to that of ^{68}Ga-TriMPyCOOHP. The study reveals that removal of one of the positive charges of the tetracationic porphyrin derivatives significantly reduces their DNA binding ability and cytotoxicity as well as brings changes in the pharmacokinetic pattern and tumor retention in small animal model.

1. Introduction

Porphyrin and its derivatives have drawn considerable attention for quite a long time owing to their interesting physicochemical and biological properties and these macrocyclic molecules have found applications in several fields such as catalysis, photo-sensitization, molecular electronics and sensors in addition to their use as anti-oxidants and anti-microbials [1–3]. Apart from these, certain porphyrin derivatives have been found to be suitable for targeted therapy of tumorous lesions [4–12]. A combination of photo-sensitizing potential along with tumor localizing property of porphyrin derivatives makes them suitable for use in photodynamic therapy (PDT). US FDA (Food and Drug Administration of United States of America) has approved the use of two porphyrin derivatives namely, Foscan® and Photofrin® (porfimer sodium) for PDT and palliative treatment of various types of cancers such as, oesophageal and non-small cell lung cancer [4–12]. Despite this, wide-spread applications of the porphyrin derivatives for the routine clinical exploitation are yet to be achieved.

One of the primary hurdles, which have deterred the pervasive usage of these agents in clinical domain, is the lipophilicity of the porphyrin core which results undue and non-specific accumulation of these agents in several non-target organs such as, lungs, liver and gastrointestinal tracks (GIT) [9–12]. Therefore, attempts have been directed to design the suitable porphyrin derivatives having reduced lipophilicity and consequently with enhanced hydrophilicity. This can be accomplished either by introducing hydrophilic moieties in the peripheral region of the porphyrin skeleton or by the introduction of positive or negative charge in the porphyrin moiety [13–16]. As lipid bi-layer of cell membrane is negatively charged, it is expected that an oppositely charged molecule will be more suitable to find its way inside the cells [13–16]. Based on these facts, an attempt was made to synthesize two cationically charged porphyrin derivatives, one tetracationic and the other tricationic, by the incorporation of pyridiniumyl moieties at meso

* Corresponding author. Radiopharmaceuticals Division, Bhabha Atomic Research Centre, Trombay, Mumbai, 400085, India.
E-mail address: tdas@barc.gov.in (T. Das).

https://doi.org/10.1016/j.ejmech.2021.113184
0223-5234/

positions of the porphyrin structure.

5,10,15,20-tetrakis(1-methylpyridinium-4-yl)porphyrin (TMPyP) is a well-studied tetracationic porphyrin derivative, with four pyridiniumyl units, whose synthesis and characterization have been previously reported by the authors in connection with their study to develop a radiolabeled porphyrin derivative for PET (positron emission tomography) imaging of tumorous lesions [10,17]. During the course of present work, authors have synthesized the same tetracationic porphyrin derivative along with a new tricationic porphyrin derivative, namely 5-carboxymethyleneoxyphenyl-10,15,20-tris(1-methylpyridinium-4-yl)porphyrin (TriMPyCOOHP) by replacing one of the pyridiniumyl moieties by carboxymethyleneoxyphenyl group (HOOC-CH_2-O-C_6H_4-) in order to study the effect of structural modification as well as variation of overall charge of the porphyrin derivatives on their tumor affinity. Both the charge bearing porphyrin derivatives were examined for their interaction with DNA (Deoxyribo Nucleic Acid), if any, by ultra violet-visible (UV–Vis) spectroscopy, isothermal titration calorimetry (ITC) as well as by *in-vitro* fluorescence cell imaging studies. Photocytotoxicity studies at two different light doses were also conducted to evaluate the possible potential of these derivatives in PDT. A comparison of *in-vivo* tumor targeting efficacy of these two derivatives was carried out in Fibrosarcoma tumor bearing Swiss mice model after radiolabeling the derivatives with ^{68}Ga. Gallium-68 [$T_{1/2} = 68$ min, $\beta^+_{(max)} = 1.89$ MeV (89%)] is a generator produced radionuclide which is widely used for PET imaging of various human ailments [18–21]. Availability from a ^{68}Ge/^{68}Ga radionuclide generator system as well as possibility of multiple elutions of ^{68}Ga in a day from this generator system are the two prime factors responsible for the wide use of ^{68}Ga for the preparation of various radiotracers for PET imaging [18–21].

In the present study, our attempts were directed towards comparing two structurally different cationically charged porphyrin derivatives for their DNA targeting ability as well as tumor affinity to understand the role played by the positive charge in the structure of porphyrin moiety with an aim to shed light on the notion that uptake of porphyrin derivatives is solely directed by their lipophilic character.

2. Experimental

2.1. Materials and methods

4-Pyridinecarboxaldehyde, tetrahydrofuran, N,N′-dimethylformamide (DMF) and Di-phenylisobenzofuran (DPBF) were procured from Sigma-Aldrich (USA). Ethyl bromoacetate, propionic acid, nitrobenzene, iodomethane, dimethylsulphoxide (DMSO), sodium hydroxide and anhydrous potassium carbonate were procured from S.D. Fine Chemicals (India). Thin Layer Chromatography (TLC) was performed using silica gel 60 F_{254} coated aluminium sheets, procured from Merck (India). Fourier Transform Infra-Red (FT-IR) spectra were recorded in a Bruker Spectrophotometer (Germany). UV–Vis spectra were recorded using LABINDIA Analytical (UV 3092) UV–Vis Spectrophotometer, while fluorescence spectra were recorded using JASCO FP-8500 Spectrofluorometer (Japan). Nuclear Magnetic Resonance (NMR) spectra were acquired using VARIAN Mercury Plus 300 MHz NMR spectrometer (USA) and Bruker 800 US, 800 MHz NMR spectrometer (Switzerland). Mass spectra were recorded using Varian 410 Prostar Binary LC Mass Spectrometer (USA) employing Electron Spray Ionization (ESI) technique. MALDI-TOF (Matrix-Assisted Laser Desorption/Ionization - Time Of Flight) Mass Spectrometry (MS) was carried out using MALDI-TOF mass spectrometer (UltrafleXtreme, Bruker, Germany).

Gallium-68 was obtained from a ^{68}Ge/^{68}Ga radionuclide generator [1.11 GBq, 30 mCi] purchased from ITG (Germany). C-18 reversed phase Sep-Pak® cartridges for purification of radiolabeled porphyrin complexes were procured from Waters (India). The High Performance Liquid Chromatography (HPLC) system (PU 1580) used for the present study was obtained from JASCO (Japan). A C-18 reverse phase HiQSil (250 × 4 mm) column was used and the elution profile was monitored by detecting the radioactivity signal using a NaI(Tl) detector coupled with the HPLC system. All the solvents used for HPLC analyses were of HPLC grade and filtered prior to use. All radioactive countings, except the countings related to the biodistribution studies, were performed using a well-type NaI(Tl) scintillation counter, manufactured by Electronic Corporation of India Limited (India). The baseline of the detector was kept at 450 keV and a window of 100 keV was used in order to utilize the 511 keV annihilation photo-peak of ^{68}Ga.

All chemicals and reagents like MTT (3-(4,5-dimethylthiazol-2-yl)-2,5-diphenyltetrazolium bromide), sodium acetate, sodium chloride, sodium bicarbonate, HEPES [(4-(2-hydroxyethyl)-1-piperazineethanesulfonic acid)], DMEM (Dulbecco's Modified Eagle Medium) media, CT-DNA (Calf Thymus - Deoxyribo Nucleic Acid) and trypan blue were procured from Sigma Chemical Inc. (USA). DAPI (4′,6-diamidino-2-phenylindole) was procured from Merck (India). Fetal Bovine Serum (FBS) was purchased from GIBCO Laboratories (USA). POLAR star Omega Plate Reader UV–Vis Spectrophotometer, obtained from BMG LABTECH (Germany), was used to measure the spectrometric readings. A549 cells were procured from National Centre for Cell Sciences (India). For photocytotoxicity experiments, cells were exposed to light generated by a set-up which included LED (Light Emitting Diode) bulbs (9 W and 14 W, Philips, India) as light source. The light doses received by the cells were measured using an irradiance meter (Megger PVM210, Taiwan) and are expressed as kJ/cm^2. Cell imaging studies were carried out in a Fluorescence Microscope (Olympus, Model: B × 53F) at 10× magnification. ITC was performed with MicroCal ITC200 system obtained from Malvern Instruments (UK).

Swiss mice (6–8 weeks age, 20–25 g weight) bearing fibrosarcoma tumors were used as animal models for the biological studies. The fibrosarcoma cell line used for raising the tumors in the animals was also purchased from National Centre for Cell Sciences (India). All the animals used for the present study were bred and reared in the laboratory animal house facility of our Institute following the standard protocol. Radioactive countings associated with the animal studies were performed using a flat-type NaI(Tl) scintillation detector, procured from Electronic Corporation of India Limited (India), employing the same counting set-up mentioned earlier. The animal studies reported in the present article were approved by the Institutional Animal Ethics Committee (IAEC) of Bhabha Atomic Research Centre (BARC) and all the animal experiments were carried out in strict compliance with the institutional (IAEC) guidelines following the relevant national laws related to the conduct of animal experimentation (Prevention of Cruelty to Animals Act, 1960).

All biological experiments were performed twice with each sample in triplicates. All data are represented as mean ± standard deviation. The differences between two groups were analyzed by using the Student's t-test. ANOVA was used for comparisons among multiple groups to compare between different pair of treatments for determining the significance value; $p < 0.05$ was considered to be statistically significant.

2.2. Synthesis and characterization of 5,10,15,20-tetrakis(1-methylpyridinium-4-yl)porphyrin (TMPyP) [2]

Tetracationic porphyrin derivative namely, 5,10,15,20-tetrakis(1-methylpyridinium-4-yl)porphyrin (**2**) was synthesized

by N-methylation of 5,10,15,20-tetra(4-pyridyl)porphyrin (**1**) following the procedure reported earlier [10]. In brief, compound (**1**) was synthesized by refluxing equimolar ratio of pyridine-4-carboxyaldehyde (4.28 g, 40 mmol) and pyrrole (2.67 g, 40 mmol) in presence of nitrobenzene (10 mL) using propionic acid (50 mL) as solvent for a period of 2 h. The reaction mixture was allowed to attain room temperature and residual solvents were removed by vacuum distillation. The solid residue, thus obtained, was washed with petroleum ether and subsequently purified by silica gel chromatography using 0.5% methanol in chloroform as the eluting solvent.

Compound (**1**): (yield = 450 mg, 2.4%). UV–Vis ($CHCl_3$, λ_{max} nm): 415, 512, 544, 587, 642. ^{1}H NMR ($CDCl_3$, δ ppm): −2.92 (2H, s, -NH), 8.18 (8H, d, J = 4.5 Hz, *m*-pyridyl-H), 8.87 (8H, s, pyrrole-H), 9.06 (8H, d, J = 5.7 Hz, *o*-pyridyl-H). ESI-MS: $C_{40}H_{26}N_8$ (calcd.) 618.69, MS (ESI^+): observed 619.8 $[M+H]^+$.
Compound (**2**): (yield = 263 mg, 80%). UV–Vis (H_2O, λ_{max} nm, log ϵ): 422 (4.39), 516 (3.59), 551 (3.41), 584 (3.40), 656 (3.29). ^{1}H NMR (DMSO, δ ppm): −3.10 (2H, s, -NH), 4.72 (12H, s, $^+$N-CH_3), 9.00 (8H, d, J = 6.6 Hz, *m*-pyridyl-H), 9.20 (8H, s, pyrrole-H), 9.47 (8H, d, J = 6.6 Hz, *o*-pyridyl-H). ESI-MS: $C_{44}H_{38}N_8$ (calcd.) 678.83, MS (ESI^+): observed $[M]^{4+}$ 169.1, $[M\text{-}CH_3]^{3+}$ 221.2, $[M\text{-}2CH_3]^{2+}$ 324.2, $[M\text{-}3CH_3]^+$ 633.2. MALDI-TOF: observed 633.339 $[M\text{-}3CH_3]^+$.

2.3. Synthesis and characterization of 5-carboxymethyleneoxyphenyl-10,15,20-tris(1-methylpyridinium-4-yl)porphyrin (TriMPyCOOHP) [5]

Synthesis of 5-carboxymethyleneoxyphenyl-10,15,20-tris(1-methylpyridinium-4-yl)porphyrin [5] was accomplished by following a three-step reaction procedure mentioned below:

2.3.1. Synthesis and characterization of 5-carboethoxymethyleneoxyphenyl-10,15,20-tris(4-pyridyl)porphyrin [3]

Compound (**3**) was synthesized by refluxing a mixture of pyrrole (5.2 mL, 0.08 mol), 4-pyridinecarboxaldehyde (5.4 mL, 0.06 mol) and *p*-carboethoxymethyleneoxybenzaldehyde (4 g, 0.02 mol) in a molar ratio of 4:3:1, in presence of nitrobenzene (10 mL), using propionic acid (40 mL) as solvent. *p*-carboethoxymethyleneoxybenzaldehyde (**1a**), used as one of the ingredients for the above-mentioned reaction, was synthesized by following a procedure reported in the literature [9]. The refluxing was continued for 2 h and the reaction mixture was allowed to attain room temperature, subsequent to which it was stored at 4 °C overnight. The residual solvent of the reaction mixture was removed by distillation. The residue, thus obtained, was extracted in chloroform followed by removal of the solvent using rotary evaporator. The desired product was purified by carrying out repeated column chromatography procedures using a maximum of 4% methanol in chloroform as the eluting solvent (R_f = 0.4). This resulted into the formation of ~250 mg of compound (**3**), which was characterized by FT-IR, UV–Vis, NMR spectroscopy and Mass spectrometry. Compound (**3**): (yield = 250 mg, 2%). UV–Vis ($CHCl_3$, λ_{max} nm, log ϵ): 414 (4.13), 511 (2.80), 545 (2.35), 588 (2.26), 643 (1.93). FT-IR ($CHCl_3$, $\bar{\upsilon}$ cm^{-1}): 3316.97, 2922.77, 1756.95, 1653.10, 1593.07, 1473.87, 1289.72, 1200.94.^{1}H NMR ($CDCl_3$, δ ppm): −2.88 (2H, s, -NH), 1.41–1.43 (3H, t, J = 7.1 Hz), 4.41–4.43 (2H, q, J = 6.7 Hz), 4.93 (2H, s), 6.91 (1H, s, pyrrole-H), 7.31–7.32 (2H, d, J = 8.4 Hz, *m*-Ar-H), 7.72 (3H, s (poorly resolved), pyrrole-H), 8.12–8.13 (2H, d, J = 8.4 Hz, *o*-Ar-H), 8.17 (6H, s, pyridyl-H), 8.85–8.87 (4H, m, pyrrole-H), 9.06 (6H, s, pyridyl-H). ^{13}C NMR ($CDCl_3$, δ ppm): 14.31 (-CH_3), 61.66 (Ph-O-CH_2), 65.73 (O-CH_2-), 113.19, 116.94, 117.40, 119.03 (>C = , methine bridges), 120.29 (*m*-Ar), 121.33 (*o*-Ar), 122.21 (β-pyrrole), 129.44 (*p*-Ar), 134.05, 134.87, 135.66 (β-pyrrole), 143.76, 148.21 (*p*-pyridine), 150.15, 150.62 (α-pyrrole), 158.06 (*m*-pyridine), 168.99 (*o*-pyridine), 184.21 (>C=O). ESI-MS: $C_{45}H_{33}N_7O_3$ (calcd.) 719.79; MS (ESI^+): observed [M+H] 720.9. MALDI-TOF: observed 720.285 [M+H].

2.3.2. Synthesis and characterization of 5-carboethoxymethyleneoxyphenyl-10,15,20-tris(1-methylpyridinium-4-yl)porphyrin [4]

Compound (**4**) was synthesized by room temperature stirring of compound (**3**) (0.1 g, 0.13 mmol) with excess of CH_3I using dichloromethane as solvent. Post-reaction, the solvent was removed by using a rotary evaporator and the residue left behind was re-dissolved in dry DMF. The solution was stirred at room temperature after the addition of excess CH_3I for a period of 24 h. Progress of the reaction was monitored by TLC using 15% MeOH in $CHCl_3$ (R_f = 0.1). Finally, the solvent was removed by rotary evaporator following repetitive washings with ether. The purified compound (**4**) was characterized by FT-IR, UV–Vis, NMR spectroscopy and mass spectrometry. Compound (**4**): (yield = 75 mg, 80%). UV–Vis (MeOH, λ_{max} nm, log ϵ): 427 (4.05), 518 (3.89), 560 (3.84), 593 (3.49), 648 (3.25). FT-IR (MeOH, $\bar{\upsilon}$ cm^{-1}): 3411.94 (MeOH), 3040.11, 1736.42, 1636.71, 1562.12, 1507.06, 1448.13, 1321.40, 1216.69, 1184.58. ^{1}H NMR (DMSO, δ ppm): −3.01 (2H, s, -NH), 1.30 (3H, t, J = 7.2 Hz), 4.27–4.30 (2H, q, J = 7.2 Hz), 4.70 (9H, s, N-CH_3^+), 5.08 (2H, s), 7.02 (2H, s, pyrrole-H), 7.41–7.42 (2H, d, J = 8.0 Hz, *m*-Ar-H), 8.14–8.15 (2H, d, J = 8.0 Hz, *o*-Ar-H), 8.39–8.40 (3H, d, J = 6.4 Hz, pyridyl-H), 8.96–8.98 (6H, m, pyrrole-H), 9.17–9.18 (3H, d, J = 6.4 Hz, pyridyl-H), 9.42–9.43 (6H, d, J = 6.4 Hz, pyridyl-H). ^{13}C NMR (DMSO, δ ppm): 14.62 (-CH_3), 48.48 (CH_3-N^+), 61.39 (Ph-O-CH_2), 65.50 (O-CH_2-), 113.90, 114.83, 115.70 (>C =, methine bridges), 121.32 (*m*-Ar), 123.18 (*o*-Ar), 126.93 (β-pyrrole), 132.60 (*p*-Ar), 133.65, 134.94, 136.02 (β-pyrrole), 144.65, 147.09 (*p*-pyridine), 150.71, 156.98, 158.45 (α-pyrrole), 162.91 (*m*-pyridine), 169.36 (*o*-pyridine), 181.92(>C=O). ESI-MS: $C_{48}H_{42}N_7O_3$ (calcd.) 764.89; MS (ESI^+): observed 254.9 $[M]^{3+}$, 374.7 $[M\text{-}CH_3]^{2+}$. MALDI-TOF: observed 734.299 $[M\text{-}2CH_3]^+$.

2.3.3. Synthesis and characterization of 5-carboxymethyleneoxyphenyl-10,15,20-tris(1-methylpyridinium-4-yl)porphyrin [5]

Compound (**5**) was synthesized by alkaline hydrolysis of compound (**4**), which was carried out by room temperature stirring of compound (**4**) (0.05 g, 0.065 mmol) in a bi-phasic solvent medium consisting of DMF and 2 N NaOH in 1:1 (v/v) ratio. The reaction was magnetically stirred for 48 h at room temperature. Post-reaction, the solvent was evaporated using a rotary evaporator and the residue left behind was treated with 2 N hydrochloric acid (HCl) followed by drying using rotary evaporator to remove the solvent. The residue thus obtained was extracted using dry methanol repeatedly so as to extract the compound (**5**) leaving behind the sodium salt. The compound (**5**), thus obtained, was characterized by FT-IR, UV–Vis spectroscopy and mass spectrometry. Compound (**5**): (yield = 43 mg, 90%). UV–Vis (H_2O, λ_{max} nm, log ϵ): 417 (3.86), 518 (3.07), 558 (3.01), 584 (2.99), 645 (2.90). FT-IR (MeOH, $\bar{\upsilon}$ cm^{-1}): 3559.77, 1637.79, 1589.05, 1378.00, 994.26. ESI-MS: $C_{46}H_{38}N_7O_3$ (calcd.) 736.84 MS (ESI^-): observed 736.6 [M]. MALDI-TOF: observed 782.610 [M+4Na-H-3CH_3].

2.4. Isothermal titration calorimetry (ITC)

For ITC, porphyrin derivatives [TMPyP (0.75 mM), TriMPyCOOHP (0.75 mM)] were prepared in 1 × TE buffer (10 mM tris, 1 mM EDTA, pH = 8). Calorimeter cell (200 μL) was loaded with CT-

DNA (0.03 mM) and the solutions of porphyrin derivatives were injected into CT-DNA until the signal saturation was achieved. Injections were performed in the sequential aliquots of 19 × 2 μL. In order to minimize the impact of equilibration artifacts, results obtained corresponding to first injection of 0.4 μL was not considered during analysis. All the titrations were performed at 25 °C. Analysis of all ITC experiments was carried out using the single site model with ITC 200 software after subtracting the buffer titrations. These isotherms were fitted with single site binding model using ITC 200 software. The model assumes the presence of independent binding sites for ligand to give stoichiometry (n), ΔH and association constant (K) of their respective interactions.

2.5. Determination of interaction of TMPyP and TriMPyCOOHP with CT-DNA by UV–Vis spectroscopy

UV–Vis spectra of TMPyP and TriMPyCOOHP as well as their mixtures with CT-DNA were recorded in tris buffer (10 mM tris, 1 mM EDTA, pH = 8) and shift in absorption maxima of Soret band was monitored, if any, by following the procedure reported elsewhere [22]. In the cuvette containing ~2 × 10^{-6} M solution of the porphyrin derivatives in tris buffer (2.0 mL), 50 μL of buffer was replaced gradually with small aliquots (50 μL) of CT-DNA (0.03 mM) and the corresponding UV–Vis spectra were recorded after 10 min of each addition. A total of 150 μL of CT-DNA was added in each cuvette. The experiment was performed similarly for both the porphyrin derivatives. Attempts were also made to analyze the interaction of TMPyP with CT-DNA by gradually increasing the CT-DNA to TMPyP ratio viz. 0.18, 0.37, 0.56, 0.75, 0.93 and 1.12 and monitoring the corresponding changes in absorption and emission spectra. Additionally, attempts were made to observe change in the absorption spectrum of TMPyP-CT-DNA solution mixture at higher buffer strength (100 mM instead of 1 mM). Absorption spectra of TMPyP-CT-DNA mixture were also analyzed after addition of different concentrations of NaCl salt (10 mM, 100 mM and 200 mM in 2 mL tris buffer) to investigate any shift in the absorption maxima (436 nm) of porphyrin-DNA complex.

2.6. Determination of singlet oxygen formation by porphyrin derivatives

Both the porphyrin derivatives (TMPyP and TriMPyCOOHP) were analyzed for their ability to produce singlet oxygen by carrying out irradiation at one of the Q-bands (516 and 518 nm, respectively) in presence of DPBF for different time points (between 30 and 540 s for TMPyP and 30–1980 s for TriMPyCOOHP). For present experiment, stock solutions of TMPyP (1 mM) and DPBF (10 mM) were prepared in DMF whereas owing to low solubility of TriMPyCOOHP in DMF, UV–Vis absorption and emission spectra for TriMPyCOOHP were recorded by preparing its stock solution (1 mM) and that of DPBF (10 mM) in DMSO. For irradiation experiment, 4 μL of each porphyrin derivative was utilized whereas 5 μL of DPBF was used in 2 mL of DMF/DMSO resulting into final concentration of porphyrin derivative and DPBF in cuvette as 2 μM and 25 μM respectively. Relative changes (decrease) in the absorption of DPBF at 325 nm was monitored at different irradiation time points to mark the transformation of DPBF to an endoperoxide which decomposes to 1,2-dibenzoylbenzene upon reaction with singlet oxygen. Results of present experiment were plotted by taking $\ln(OD_t/OD_0)$ as Y-axis and time of irradiation (in seconds) as X-axis, where OD_t = optical density after 't' time of irradiation and OD_0 = optical density without irradiation.

2.7. Cytotoxicity assays

For cytotoxicity assays, A549 cells were cultured in DMEM medium containing 10% FBS and grown up to 60–70% confluence. After harvesting, 1 × 10^5 cells were seeded in 12-well tissue culture plates and allowed to attach to the plate overnight. Thereafter, A549 cells were treated with different concentrations of porphyrin derivatives (TMPyP and TriMPyCOOHP) viz. 0.05, 1, 10, 50, 100 μM and were incubated for various time intervals for different assays. Control set of cells were left untreated. All treatments were carried out in triplicates.

2.8. MTT assay

MTT assay is a colorimetry based technique used to measure cellular metabolic activity and thus provides information regarding the cell viability. Viable cells that contain NAD(P)H-dependent oxidoreductase enzymes reduce the MTT reagent to formazan and generate a deep purple coloration, while non-viable cells fail to produce any color change. For carrying out MTT assay, 50 μL of A549 cells (~0.5 × 10^5 cells) were harvested in serum free media, treated with different concentrations of porphyrin derivatives and incubated at 37 °C for 3 h after mixing with 50 μL of MTT solution (5 mg/mL in PBS). After incubation, 150 μL of MTT solvent (4 mM HCl, 0.1% NP40 in isopropanol) was added and incubated for 15 min under shaking condition for dissolution of formazan. Reaction was stopped by adding 1/10 volume of 1 N HCl and the absorbance of the reaction mixtures was monitored at 590 nm. Percent cell viability was calculated from these data [ratio of ODs (optical density) of treated to control sample, multiplied by 100] to find out the magnitude of cell proliferation. This data was used to plot percentage cell proliferation at different concentrations for both the porphyrin derivatives.

2.9. Trypan Blue Exclusion Viability assay

Trypan blue exclusion assay was carried out to determine the cell viability wherein the intact cells appear transparent while the dead cells take up the trypan blue dye and appear blue when viewed under the microscope. For this assay, 10 μL of 0.4% trypan blue solution was mixed with 10 μL of A549 cells (~1 × 10^4 cells) and treated with different concentrations of the porphyrin derivatives. The samples were counted for viability using a hemocytometer.

2.10. Determination of photo-cytotoxicity of TMPyP and TriMPyCOOHP by MTT assay in A549 cell lines

Photo-cytotoxicity of TMPyP and TriMPyCOOHP was determined in A549 cancer cell lines by following the procedure mentioned below. Three different cell experiments were set up. In the first set, cells were incubated with the porphyrin derivative (1 μM) in absence of light and designated as 'vehicle control-1 (Vcontrol-1)', while in second set, cells were incubated in presence of light, but without the porphyrin derivative and was designated as 'vehicle control-2 (Vcontrol-2)'. On the other hand, in third set of experiment, cells were exposed to light in presence of 1 μM of either TMPyP or TriMPyCOOHP and were designated as 'treated'. Cells were exposed to light corresponding to two different light doses viz. 0.01 and 0.04 kJ/cm^2. The irradiation was continued for 90 min and light dose received by the cells was calculated by multiplying the light intensity (in W/m^2) with time of exposure. Vcontrol-1 and treated set were incubated with TMPyP and TriMPyCOOHP for 6 h and subsequently treated set was exposed to light. The treated cell lines were incubated for another 18 h post-

irradiation. Cells were harvested for determining the cytotoxicity in presence of light by MTT and Trypan Blue Exclusion Viability assay as mentioned earlier and data for % viability was plotted for both the porphyrin derivatives at two light doses.

2.11. Cellular imaging by fluorescence

A549 cells (~0.4 × 10^6 cells) were cultured in DMEM containing 10% fetal bovine serum and 1% penicillin and streptomycin in a humidified CO_2 (5%) incubator at 37 °C. For cell uptake studies, A549 cells were plated in 6-well plate format and cultured to 70–80% confluence. Cells were treated with 10 μM concentration of either TMPyP or TriMPyCOOHP for 4–5 h. Subsequently, cells were washed gently with PBS and fixed with 4% paraformaldehyde in PBS for 15–20 min at room temperature. Cells were again washed with PBS and permeabilized with 0.1% Triton × 100 for 10 min and then stained with DAPI (5 μg/mL) for 5–10 min. Fluorescence images of A549 cells incubated with porphyrin and those stained with DAPI were captured on fluorescence microscope.

2.12. Preparation of ^{68}Ga-TMPyP and ^{68}Ga-TriMPyCOOHP

Porphyrin derivatives, namely TMPyP and TriMPyCOOHP were radiolabeled with ^{68}Ga by following a generalized procedure. Freshly eluted $^{68}GaCl_3$ (74 MBq, 2 mCi, 200 μL), obtained by eluting a ^{68}Ge/^{68}Ga generator using 0.05 N HCl, was added to 0.5 mg of TMPyP (0.808 μmol) or TriMPyCOOHP (0.679 μmol) dissolved in milliQ water (0.5 mL). The pH of the reaction mixture was adjusted to 5.5 using 2 N aqueous sodium acetate solution prior to its incubation in a boiling water bath for 30 min. Post-incubation, an aliquot of reaction mixture (5–10 μL) was injected in a RP-HPLC to determine the percentage radiochemical yield (% RCY). For further purification, ^{68}Ga-labeled porphyrin derivatives (^{68}Ga-TMPyP and ^{68}Ga-TriMPyCOOHP) were separately loaded on a C-18 reversed phase Sep-Pak® cartridge. The cartridge was pre-conditioned by passing 4.0 mL of ethanol followed by 2.0 mL of double distilled water prior to the loading of the radiolabeled preparations. Free $GaCl_3$ was eluted using 6.0 mL of double distilled water and subsequently radiolabeled porphyrin complex was eluted out from the column using 1.0 mL of ethanol. Ethanol present in the purified preparation was removed by gentle warming and the preparation was reconstituted with normal saline. The radiochemical purity of the purified ^{68}Ga-labeled porphyrins was determined by HPLC studies employing gradient elution technique following the quality control method reported elsewhere [10].

2.13. Determination of partition coefficient (log $P_{o/w}$)

Partition coefficients of ^{68}Ga-TMPyP and ^{68}Ga-TriMPyCOOHP complexes were determined in octanol-water solvent system in order to ascertain their lipophilicity/hydrophilicity. For this, the radiolabeled preparation (100 μL) was added to a mixture of water (900 μL) and octanol (1 mL) and the resulting solution was vortexed thoroughly. This mixture was subsequently centrifuged at 4000 rpm for 5 min. Aliquots of 100 μL were withdrawn from both water and octanol layers and counted separately using the well-type NaI(Tl) counter. Partition coefficient of the ^{68}Ga-labeled porphyrin derivatives were calculated from this data.

2.14. Bio-distribution studies

Pharmacokinetic evaluation of ^{68}Ga-labeled porphyrin derivatives was carried out by bio-distribution studies in fibrosarcoma bearing Swiss mice. For creating the tumors on the animals, about 10^6 cells of HSDM1C1 murine fibrosarcoma (100 μL) were injected subcutaneously on the dorsum of each animal. The tumors were allowed to grow until the size of the tumors reached about 10 mm in diameter, subsequent to which the animals were used for the experiment. Each animal, weighing 20–25 g, was intravenously injected with 100 μL of the radiolabeled preparation (~50 μCi, 1.85 MBq) through one of the lateral tail veins. Biological distribution of both the radiolabeled complexes was studied at two different post-administration time points viz. 30 and 60 min. Three animals were used for each time point. The animals were sacrificed at the designated post-administration time points through CO_2 asphyxia. Blood samples of the animals were collected by cardiac puncture immediately after sacrificing the animals. Subsequently, the organs/tissues were excised, washed with normal saline, dried, weighed in a weighing balance and radioactivity associated with each organ/tissue was measured using a flat-type NaI(Tl) counter. The percentage of injected activity (%IA) accumulated in various organs/tissue was calculated from the above data and expressed as %IA per g (%IA/g) of organ/tissue. The total activity accumulated in blood, skeleton and muscles were calculated by considering 7, 10 and 40% of the animal body weight are constituted by these organs/tissue, respectively [23,24]. Percentage of activity excreted through urine was calculated by subtracting the activity accounted for all the organs from the total injected activity.

3. Results

3.1. Syntheses and characterization of porphyrin derivatives

Both the porphyrin derivatives were synthesized by following Alder-Longo method, a commonly adopted procedure used for the synthesis of porphyrin derivatives [25] (Schemes 1 and 2).

UV–Vis spectra consisting of one intense Soret band at 418–422 nm followed by four less intense Q-bands in between 500 nm and 700 nm along with a signal corresponding to two protons in the negative region of ^{1}H NMR spectra provided conclusive evidence in favour of the formation of porphyrin moiety in various porphyrin derivatives synthesized in the present study. Presence of an ester group in the porphyrin structure (**3**) was confirmed by the presence of the peak at 1756.95 cm^{-1} in FT-IR spectrum. Its formation was further confirmed by the presence of a mass peak at 720.285 (obtained using MALDI-TOF instrument) corresponding to molecular ion [M+H]. Mass spectra of compounds (**2**) and (**4**) recorded in positive mode (ESI-MS), exhibited *m*/*z* peaks at 169.1 $[M]^{4+}$ and 254.9 $[M]^{3+}$ respectively, whereas 633.339 $[M\text{-}3CH_3]^+$ and 734.299 $[M\text{-}2CH_3]^+$ were the most abundant peaks corresponding to compound (**2**) and (**4**) in the mass spectra acquired using MALDI-TOF mass spectrometer, indicating the formation of tetracationic and tricationic molecular ions respectively providing an evidence in favour of the formation of four and three quaternary nitrogen centres, respectively. FT-IR spectrum of compound (**5**), obtained by basic hydrolysis of compound (**4**), exhibited peaks characteristic to -OH and >C=O of carboxylic group at 3559.77 (broad) and 1637.79 cm^{-1}, respectively. Observation of a sharp singlet at 4.72 ppm corresponding to 12 protons arising from the methyl groups attached with quaternary nitrogen centre in ^{1}H NMR spectrum of compound (**2**) confirmed the methylation of all the four pyridyl nitrogens present in the porphyrin structure. Symmetrical structure of compound (**2**) resulted into a singlet for all the eight hydrogens of pyrrole rings. Similarly, eight hydrogens each at ortho- and meta-positions of pyridine rings exhibited two doublets in the ^{1}H NMR spectrum. In ^{1}H NMR spectrum of compound (**3**), observation of a triplet, quartet and singlet at chemical shift positions of 1.42 ppm, 4.42 ppm and 4.93 ppm, respectively provided evidence in favour of presence of an aliphatic chain (-O–CH_2–COO–CH_2–CH_3) in its structure. Additionally, presence

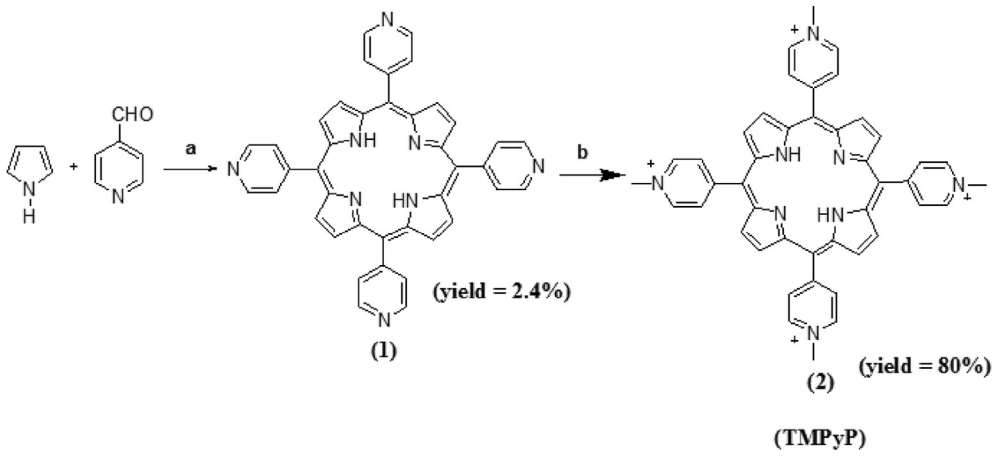

Scheme 1. Reaction scheme for the synthesis of compound TMPyP (**2**): (a) nitrobenzene, propionic acid, reflux, 2 h; (b) CH_3I, RT, Stirring for 48 h.

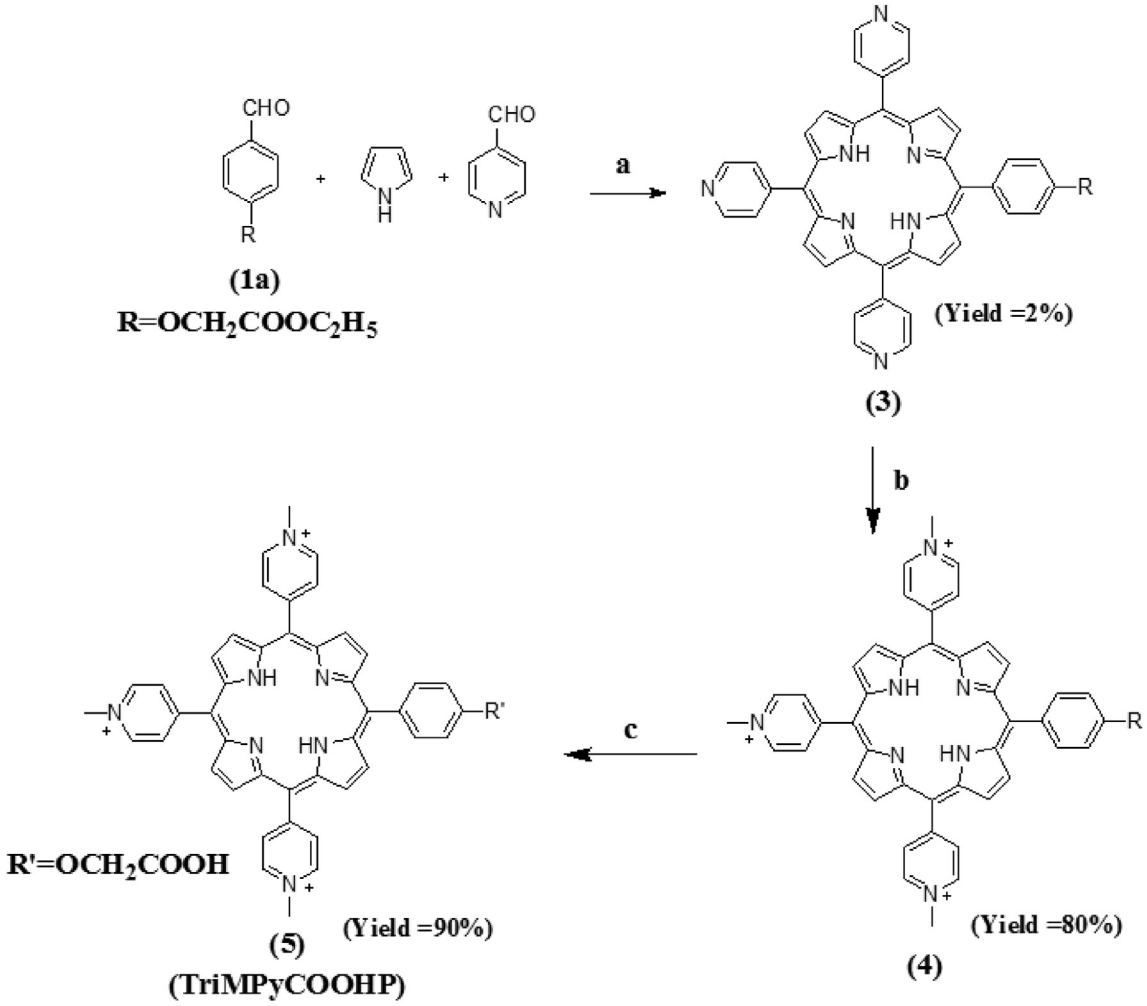

Scheme 2. Reaction scheme for the synthesis of compound TriMPyCOOHP (**5**): (a) nitrobenzene, propionic acid, reflux, 2 h; (b) CH_3I, RT, Stirring for 48 h; (c) DMF:2 N NaOH (1:1 v/v), RT, Stirring for 48 h.

of carbonyl ester carbon [single such carbon in compound (**3**)] was confirmed by ^{13}C NMR spectroscopy where a peak at chemical shift of 184.21 ppm was observed. Methylation of nitrogen in all the three pyridyl rings, present in the structure of compound (**4**), leading to formation of three cationic centres, was confirmed by presence of a sharp singlet corresponding to nine hydrogens at

4.44 ppm in ^{1}H NMR spectrum. Ortho and meta-hydrogens of a single benzene ring present in the structure of compound (**4**) exhibited two doublets at 7.42 and 8.14 ppm corresponding to integration for two hydrogens each. Due to insertion of cationic centres in the structure of compound (**4**), chemical shifts corresponding to hydrogens attached to pyridyl carbons including others in the aromatic region were observed to be shifted downfield relative to those present in the structure of compound (**3**). Similar observation was also made in ^{1}H NMR spectra obtained for compound (**1**) and (**2**).

3.2. Isothermal titration calorimetry (ITC)

ITC measurements were carried out to understand thermodynamics of porphyrin and CT-DNA interaction for both the porphyrin derivatives. The interaction between TMPyP and CT-DNA was found to be exothermic, which is evident from negative value of the enthalpy observed when TMPyP was allowed to interact with CT-DNA (Fig. 1). Saturation of binding sites on DNA was achieved after eleven injections. The isotherm obtained by plotting heat change vs. molar ratio (porphyrin and CT-DNA) was used to calculate stoichiometry (n), change of enthalpy (ΔH), change of entropy (ΔS) and association constant (K) of TMPyP-DNA binding (Fig. 1). These values were found to be similar to those reported in the literature [22]. On the other hand, injections of TriMPyCOOHP into CT-DNA resulted in insignificant amount of heat signatures as compared to TMPyP-CT-DNA interaction, which indicated absence of interaction between TriMPyCOOHP and CT-DNA.

3.3. Determination of interaction of TMPyP and TriMPyCOOHP with CT-DNA by UV–Vis spectroscopy

UV–Vis spectra of TMPyP and TriMPyCOOHP as well as their reaction mixtures with CT-DNA recorded in tris buffer revealed a bathocromic shift of ~14 nm for Soret band (436 from 422 nm) corresponding to the reaction mixture of TMPyP with CT-DNA (Fig. 2(a)). However, no change in absorption maxima of Soret band in UV–Vis spectrum was observed when TriMPyCOOHP was allowed to react with CT-DNA. This observation also indicated the absence of any interaction between TriMPyCOOHP and CT-DNA. Further investigation of effect on absorption and emission behavior of TMPyP-CT-DNA complex at different molar ratio (CT-DNA to TMPyP) revealed no further shift in the absorption maxima except for decrease in the absorption (hypochromicity), whereas in the corresponding emission spectra an increase in the emission intensity (hyperchromicity) was observed both at 654 nm as well as at shoulder emission of 714 nm (Fig. 2(b) and (c)). Attempts to carry out the similar studies using higher buffer strength (100 mM) revealed no significant difference with the observations made earlier when tris buffer of relatively lower strength (10 mM) was

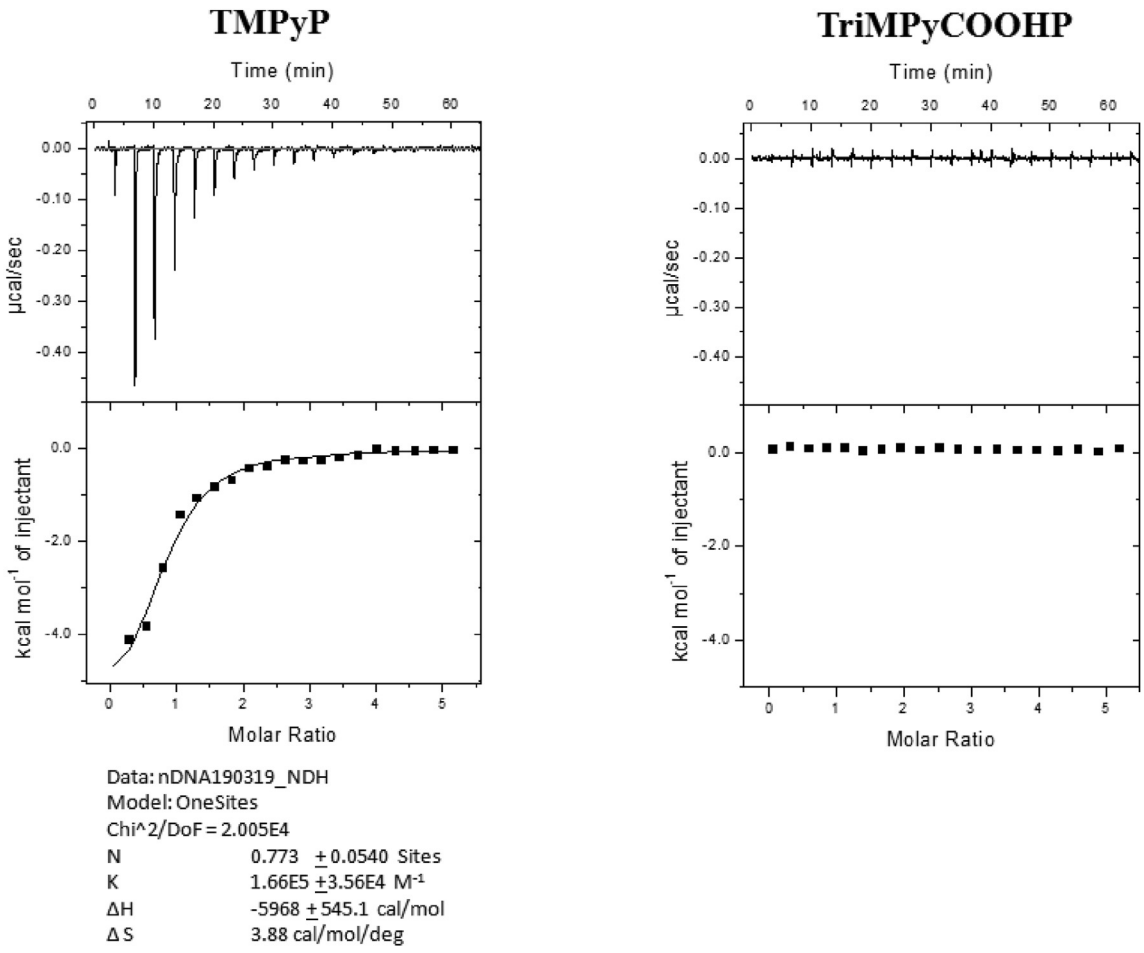

Fig. 1. ITC analysis of porphyrin-CT-DNA interaction. Upper panels depict the raw calorimetric data of the titration of TMPyP (0.75 mM) and TriMPyCOOHP (0.75 mM) into CT-DNA (0.03 mM) at 25 °C in the 1 × TE buffer (10 mM tris, 1 mM EDTA, pH = 8), whereas lower panels show the corresponding buffer corrected integrated injection heats.

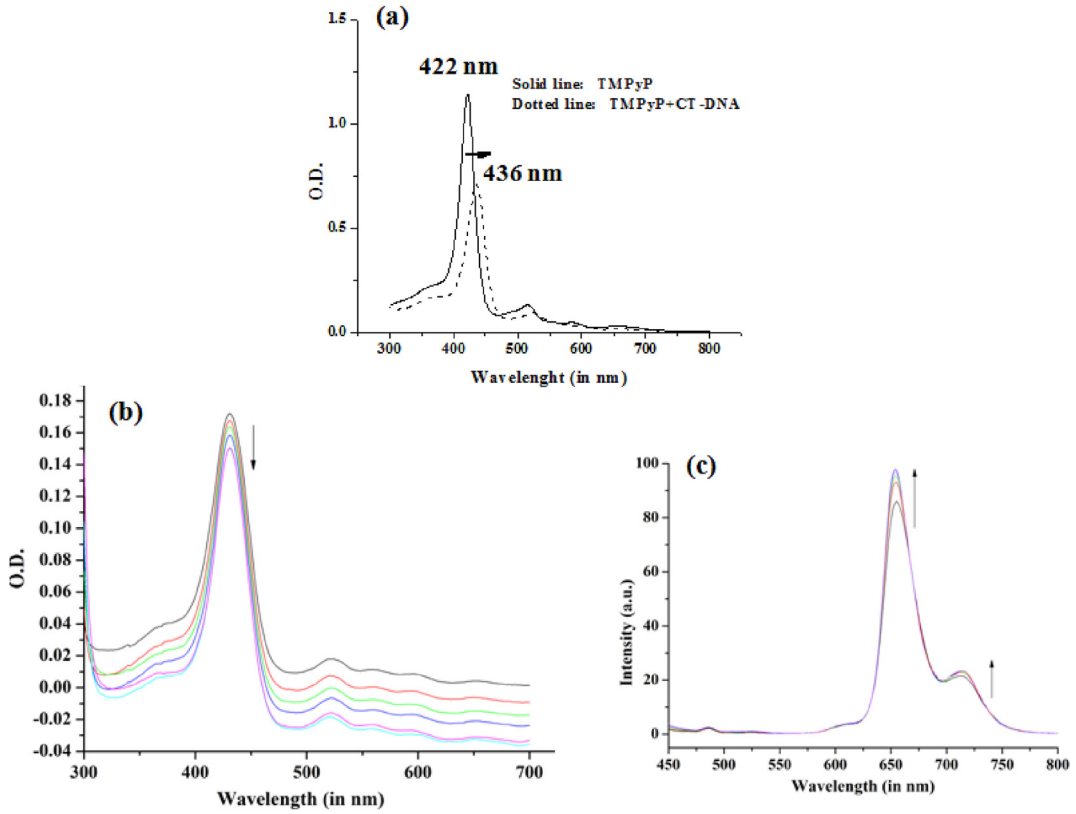

Fig. 2. Graphs: (a) Overlaid UV–Vis spectra of TMPyP (2 μM) and TMPyP-CT-DNA reaction mixture depicting bathochromic shift; (b) Overlaid absorption pattern obtained corresponding to TMPyP-CT-DNA mixture examined at different CT-DNA to TMPyP molar ratios viz. 0.18, 0.37, 0.56, 0.75, 0.93 and 1.12; (c) Overlaid emission spectra of TMPyP-CT-DNA reaction mixtures depicting rise in emission intensity with increasing CT-DNA to TMPyP molar ratios.

utilized for such studies. Additionally, attempts to study the effect of presence of salt on interaction behavior of TMPyP and CT-DNA revealed no effect on the position of the absorption maxima, confirming the well-observed mode of interaction between the two as intercalative rather than external groove binding [26,27].

3.4. Determination of singlet oxygen formation by porphyrin derivatives

Both the porphyrin derivatives were analyzed for their ability to form singlet oxygen indirectly by monitoring the decomposition of DPBF leading to decrease in the absorption of the latter upon irradiation at a wavelength specific to porphyrin derivative (Figs. 3 and 4). Graphs plotted between $\ln(OD_t/OD_0)$ and time of irradiation (in seconds) for TMPyP and TriMPyCOOHP revealed the requirement of longer periods of irradiation to observe appreciable decline in absorbance for latter than the former, which clearly indicates the relatively higher potential of TMPyP towards generation of singlet oxygen compared to TriMPyCOOHP. This observation also corroborates the results obtained during photo-cytotoxicity experiments

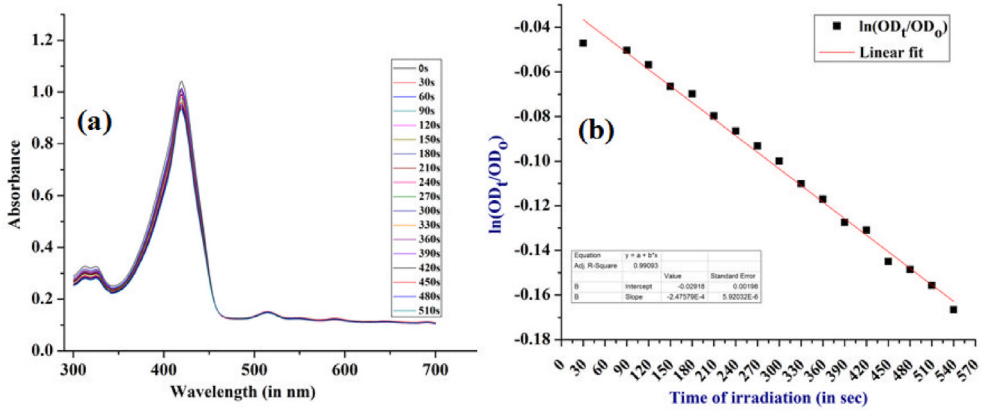

Fig. 3. Graphs (a) and (b) depicting variation in absorption at a wavelength specific to DPBF (325 nm) in presence of TMPyP (2 μM) upon irradiation at different time points ranging from 30 to 540 s.

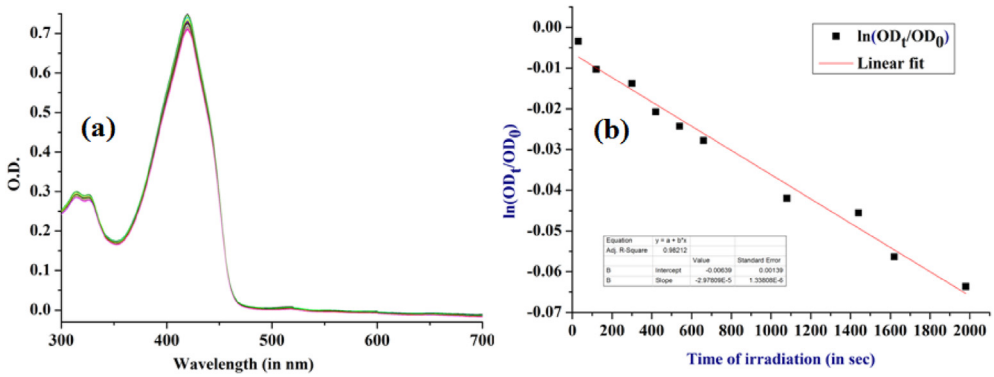

Fig. 4. Graphs (a) and (b) depicting variation in absorption at a wavelength specific to DPBF (325 nm) in presence of TriMPyCOOHP (2 μM) upon irradiation at different time points ranging from 30 to 1980 s.

(described below) where TMPyP induced greater cell death when exposed to similar radiation doses compared to that of TriMPyCOOHP.

3.5. Cytotoxicity and photo-cytotoxicity experiments

Cytotoxicity experiments carried out in A549 cancer cell line revealed the non-toxic nature of both the porphyrin derivatives towards A549 cells at the lowest tested concentration i.e. 0.05 μM (Fig. 5). However, cytotoxicity caused by both the porphyrin derivatives in absence of light was found to be increasing proportionately with the increasing concentration of the porphyrin derivatives and at highest tested concentration (100 μM), cell proliferation was observed to be reduced down to less than 50%. Moreover, TMPyP was observed to exhibit comparatively higher cytotoxicity than TriMPyCOOHP at lower concentrations ($p < 0.05$). Nonetheless, at higher concentrations, percentage cell proliferation was observed to be similar for both the porphyrin derivatives ($p > 0.05$) (Fig. 5).

Photo-cytotoxic experiments revealed the light dependent cytotoxic effects of both the porphyrin derivatives on A549 cells (Fig. 6). In comparison to both Vcontrol-1 as well as Vcontrol-2, treated set of cell lines exhibited lesser percentage of cell proliferation at both the light doses. Here again TMPyP exhibited relatively higher photo-cytotoxicity than TriMPyCOOHP when exposed to two different light doses (47.71 ± 0.71 and 43.98 ± 0.42 versus 77.67 ± 0.98 and 61.30 ± 4.59% cell proliferation at 0.01 and 0.04 kJ/cm^2 light doses, respectively) (Fig. 6) indicating the relatively higher potency of the former derivative.

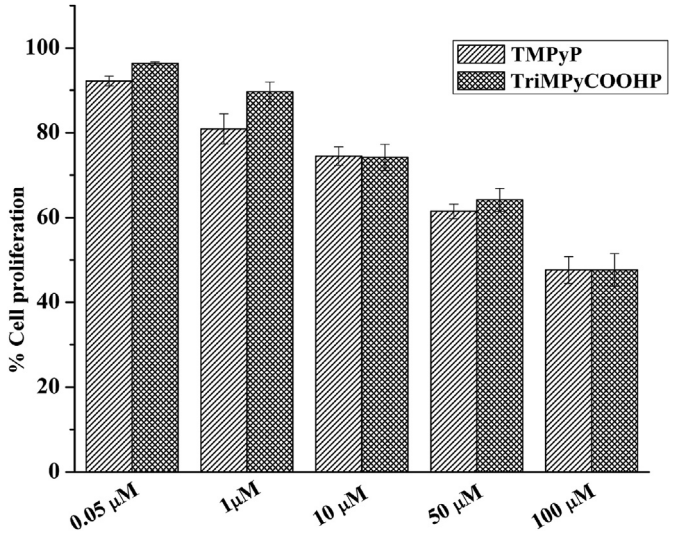

Fig. 5. Graphical representation of dark toxicity in terms of percentage cell proliferation (with respect to control) at varying concentration of TMPyP and TriMPyCOOHP obtained by MTT assay in A549 cell lines.

3.6. Cellular imaging by fluorescence

Attempts towards fluorescence imaging of TMPyP and TriMPyCOOHP in A549 cancer cell lines revealed the preferential cell uptake exhibited by TMPyP over that of TriMPyCOOHP (Fig. 7). Also, ability of the former to accumulate in cell nucleus was confirmed by merging the cell images corresponding to TMPyP and that of DAPI.

3.7. Preparation of ^{68}Ga-TMPyP and ^{68}Ga-TriMPyCOOHP

Both the porphyrin derivatives were radiolabeled with ^{68}Ga, eluted from a ^{68}Ge/^{68}Ga radionuclide generator and the maximum radiolabeling yield achieved under the optimized reaction conditions were 85.54 ± 0.52% and 70.30 ± 1.50% for ^{68}Ga-TMPyP and ^{68}Ga-TriMPyCOOHP, respectively. Therefore, attempts were made to purity the radiolabeled porphyrin derivatives using preconditioned C18-Sep-pak® cartridge columns. Post-purification, ^{68}Ga-TMPyP could be obtained with >90% radiochemical purity, while the same for ^{68}Ga-TriMPyCOOHP improved to >95%. Percentage radiochemical purity of the radiolabeled preparations were determined using HPLC radio-chromatograms, where free $^{68}GaCl_3$ eluted with a retention time (R_t) of 3.5 ± 0.24 min, whereas both the ^{68}Ga-labeled porphyrin complexes exhibited almost similar retention time of ~8.0 min (Fig. 8).

3.8. Determination of partition coefficient (log $P_{o/w}$)

Partition coefficients of ^{68}Ga-TMPyP and ^{68}Ga-TriMPyCOOHP complexes were observed to be −4.30 and −1.55, respectively indicating hydrophilic nature of both the complexes. However, it is evident from the results that the former radiolabeled complex is relatively more hydrophilic than the latter one.

3.9. Bio-distribution studies

Bio-distribution studies carried out in fibrosarcoma bearing animal model revealed to some extent differential pharmacokinetic behavior for the two ^{68}Ga-labeled porphyrin derivatives (Fig. 9). Out of the two time points chosen for animal studies viz. 30 and 60 min, it was at the higher time point where differential uptake in

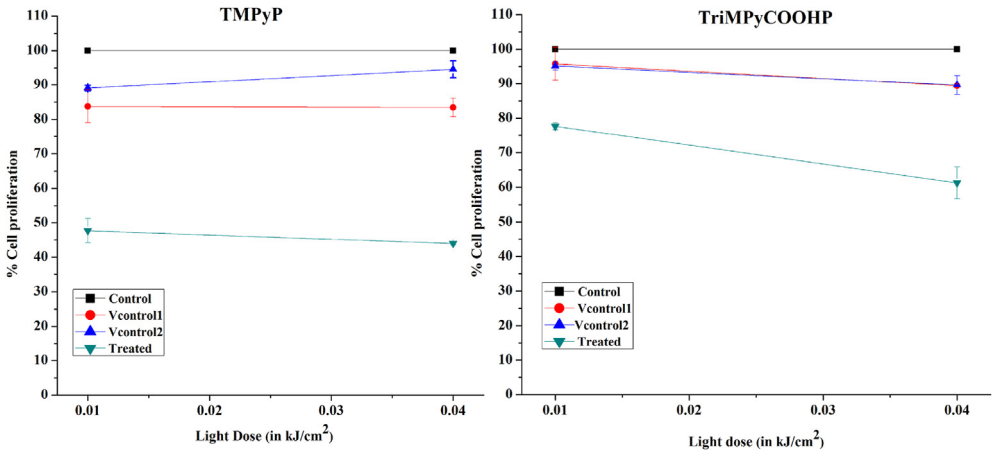

Fig. 6. Graphical representation of cell toxicity (with respect to control) exhibited by 1 μM of TMPyP and TriMPyCOOHP in A549 cell lines at two different light doses viz. 0.01 and 0.04 kJ/cm^2 ('Control' as cells without porphyrin and without light exposure, 'Vcontrol1' as cells with porphyrin and without light exposure, 'Vcontrol2' as cells without porphyrin and exposed to light, while 'treated' as cells with porphyrin and exposed to light) obtained by MTT assay.

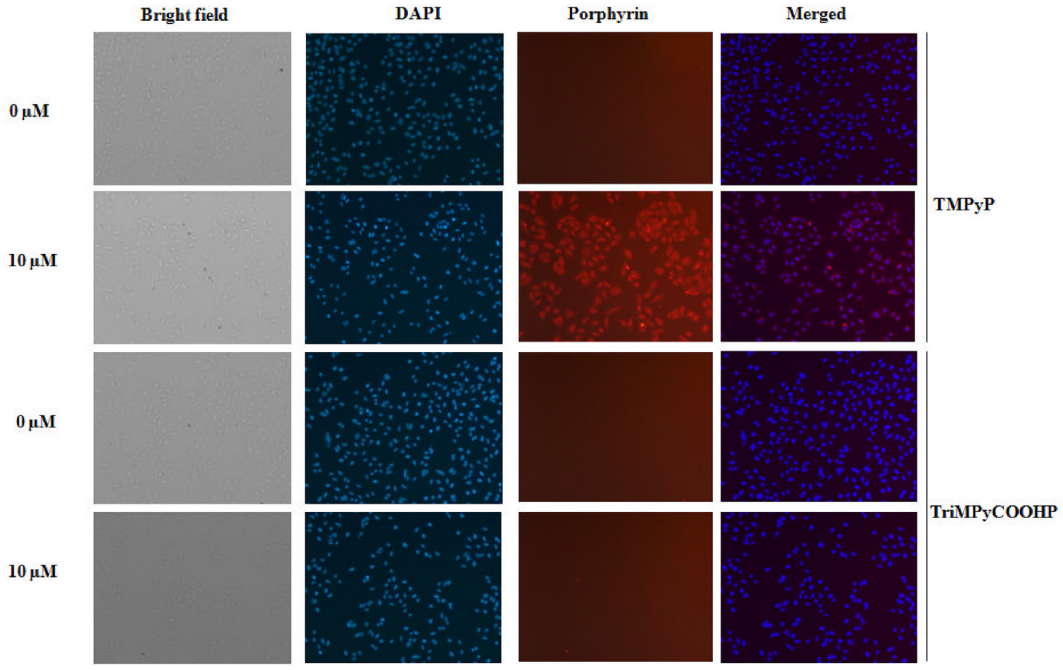

Fig. 7. Bright field and fluorescence images of A549 cells (~0.4 × 10^6 cells) incubated with DAPI (5 μg/mL), porphyrin derivatives (10 μM) and co-incubated with DAPI and porphyrin derivatives.

various organs was observed between the two radiolabeled complexes. Uptake of ^{68}Ga-TriMPyCOOHP in liver (6.39 ± 1.06 and 9.41 ± 1.71% IA/g at 30 and 60 min post-administration, respectively) at both the time points was relatively higher that was observed for ^{68}Ga-TMPyP (4.80 ± 0.18 and 3.47 ± 0.51% IA/g at 30 and 60 min post-administration, respectively) (Fig. 9). This observation can be supported by the partition coefficient values observed for both the complexes where the former complex was found to be relatively less hydrophilic than that of latter. Initially accumulated activity from various organs underwent clearance both via hepatobiliary as well as renal pathway, though clearance via latter route was observed to be predominant in case of ^{68}Ga-TMPyP (15.31 ± 0.56% IA/g at 60 min post-administration) than that observed in case of ^{68}Ga-TriMPyCOOHP (8.10 ± 0.31% IA/g at 60 min post-administration). Similar uptake in tumor mass was observed for both the complexes at early post-administration time point (6.47 ± 0.87 versus 5.34 ± 0.73% IA/g). However, at higher post-administration time point, ^{68}Ga-TMPyP exhibited significantly higher ($p < 0.05$) retention (6.07 ± 0.03 %IA/g at 60 min post-administration) compared to that of ^{68}Ga-TriMPyCOOHP (2.09 ± 1.20 %IA/g at 60 min post-administration).

This has been reflected in the resulting tumor to blood and tumor to muscle ratios as these values for ^{68}Ga-TMPyP (1.80 ± 0.14 and 9.34 ± 1.10, respectively at 60 min post-administration) are significantly higher than those for ^{68}Ga-TriMPyCOOHP complex (0.49 ± 0.23 and 4.43 ± 0.97 respectively at 60 min post-administration) (Table 1). However, high tumor to muscle ratio observed for both the complexes at all the time points indicated about their preferential ability to accumulate in the tumorous lesion (Table 1).

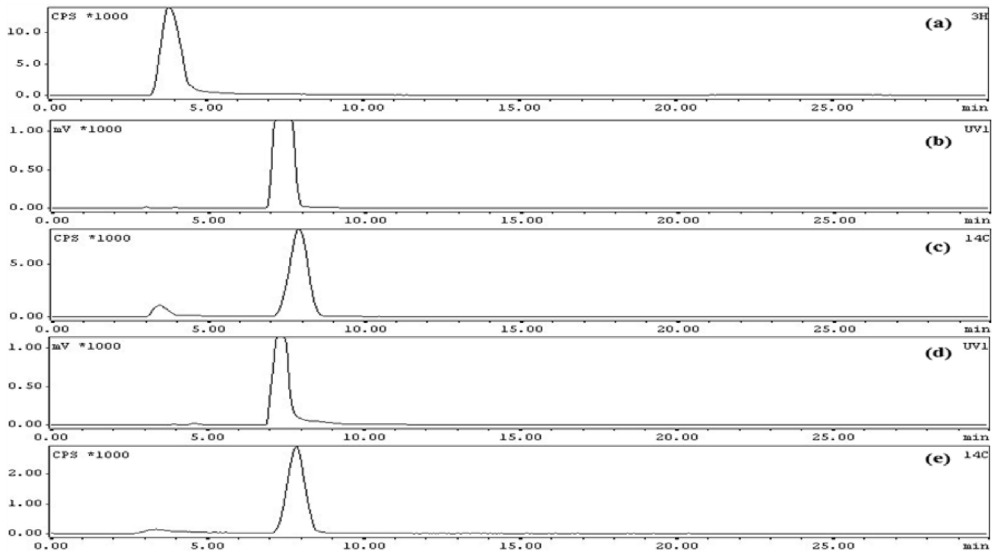

Fig. 8. HPLC profiles of (a) unlabeled/free $^{68}GaCl_3$, (b) TMPyP, (c) ^{68}Ga-TMPyP, (d) TriMPyCOOHP, and (e) ^{68}Ga-TriMPyCOOHP.

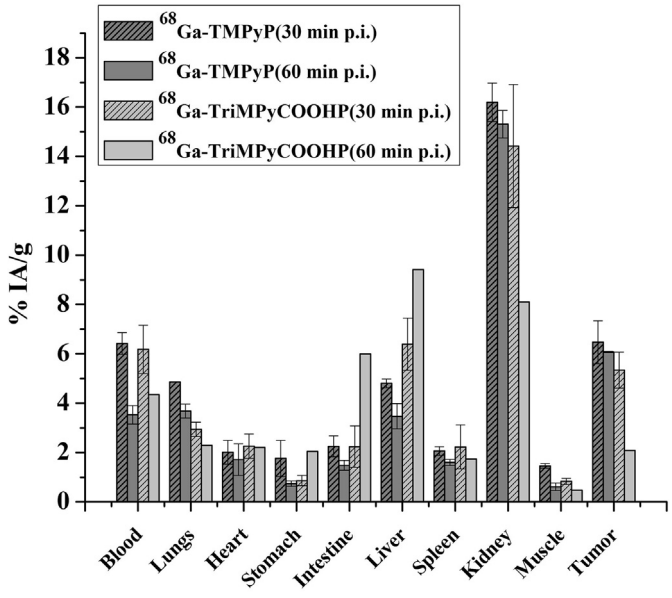

Fig. 9. Graphical representation of results of bio-distribution studies of ^{68}Ga-TMPyP and ^{68}Ga-TriMPyCOOHP carried out in fibrosarcoma bearing Swiss mice at two different post-administration time points viz. 30 and 60 min.

Table 1
Tumor to blood and tumor to muscle ratio values for ^{68}Ga-TMPyP and ^{68}Ga-TriMPyCOOHP at two different post-injection time points viz. 30 and 60 min.

Tumor/Organ ratio	^{68}Ga-TMPyP		^{68}Ga-TriMPyCOOHP	
	30 min	60 min	30 min	60 min
Tumor/Blood	0.89 ± 0.04	1.80 ± 0.14	0.86 ± 0.29	0.49 ± 0.23
Tumor/Muscle	4.41 ± 0.62	9.34 ± 1.10	6.43 ± 0.97	4.43 ± 0.97

4. Discussion

Two cationically charged porphyrin derivatives were synthesized following multi-step reaction procedures and characterized by employing standard spectroscopic techniques such as, UV–Vis, FT-IR, ^{1}H NMR, ^{13}C NMR spectroscopy as well as by mass spectrometry. Out of the two porphyrin derivatives, one is a symmetrically substituted tetracationic porphyrin (TMPyP), while the other one is the functionally modified version of first one containing three cationic centres and one aliphatic carboxylic moiety at the peripheral position (TriMPyCOOHP). The very first step of synthesis involving formation of tetrapyrrolic cavity of porphyrin is a limiting reaction with respect to yield of the desired reaction product. In case of compound (**2**) (TMPyP), it was 2.4%, whereas for compound (**3**) it was observed to be only 2%. However, lower yield of porphyrin core formation reactions is a quite common observation, especially for polar porphyrin derivatives, as they exhibit relatively lesser tendencies towards crystallization [25,28]. Despite the careful selection of stochiometric ratios of all the ingredients, formation of various other porphyrin derivatives of all possible combinations with meso-substituents was observed along with the formation of tar like polypyrrole products during the course of syntheses of the porphyrin derivatives reported in the present study [25,28]. However, once porphyrin core is formed, rest of the reactions involving participation of meso-substituents resulted into relatively higher yields.

It is well-documented in the literature that porphyrins have an inherent tendency to accumulate in the tumorous lesions [4–12] and interact with duplex DNA as well as G-quadruplexes, which are well-known structural elements of telomeres as well as promoters of certain pro-oncogenes [22]. Therefore, interaction of porphyrin with G-quadruplex can potentially abrogate DNA-telomerase interaction and mitigate the expression of important oncogenes [22]. In this line, the present work involves the attempts made to carry out the comparative evaluation of two in-house synthesized porphyrin derivatives (TMPyP and TriMPyCOOHP) towards accumulation in tumorous lesions and more precisely, studying the effect of removing one charged centre and replacing the same with an aliphatic carboxylic acid moiety on DNA-porphyrin interaction. The rationale behind carrying out the aforementioned modification was due to the fact that porphyrin-based ligands are used for targeting mostly solid tumors and such tumors usually have slightly acidic microenvironment owing to the enhanced formation of lactic acid [29]. Aliphatic carboxylic acids have a pKa of ~5.0 and at physiological pH (i.e. in blood stream), it is expected to remain in carboxylate ion form. However, after penetration through the cell

membrane, it is expected that the porphyrin derivative will undergo protonation and will be retained within the cell in the protonated form [29]. Therefore, to enhance the probability of cellular penetration and retention, carboxylic acid derivative of phenyl residue was chosen while designing the structure of TriMPyCOOH.

Both the porphyrin derivatives were screened for possible interaction with CT-DNA by performing various experiments. As revealed in ITC experiments, TMPyP exhibited binding with CT-DNA which was reflected in the values of thermodynamic parameters such as, association constant (K), stoichiometry (n), enthalpy (ΔH) and entropy (ΔS) associated with the reaction ($K = 16.60 \pm 3.56 \times 10^4\ M^{-1}$, $N = 0.77 \pm 0.05$, $\Delta H = -5.96 \pm 0.54$ kcal mol^{-1}, $\Delta S = 3.88$ cal mol^{-1} deg^{-1}). The thermodynamic data obtained in the present case is found to be strikingly similar to that of interaction of TMPyP with G2-quadruplex reported elsewhere [22]. However, it is interesting to note that TriMPyCOOHP failed to exhibit any such interaction. These observations were also corroborated by UV–Vis spectroscopy where interaction of CT-DNA with TMPyP resulted a bathochromic shift of the Soret band by ~14 nm (436 from 422 nm), but no such shift of the Soret band was observed when CT-DNA was allowed to interact with TriMPyCOOHP. This observation also indicates minimal or no interaction between the tricationic porphyrin derivative with DNA. This observation infers that such structural modification of the porphyrin moiety has a detrimental effect with respect to its DNA-interacting capability. Further investigations of interaction between TMPyP and CT-DNA at higher DNA/TMPyP molar ratios revealed serial increase in the fluorescence intensity, which is indicative of the phenomenon where electrostatic interaction of TMPyP with DNA promotes quenching of S^1 state (first singlet excited state) of the photosensitizer and promotes fluorescence ('on state' of photosensitizer) [30].

In agreement with the previous observations, during fluorescence imaging studies, TMPyP was observed to exhibit accumulation in the nucleus of A549 cells, which was further confirmed by co-incubation with DAPI; whereas TriMPyCOOHP failed to exhibit similar behavior. Cell cytotoxicity studies in dark as well as in presence of light carried out by two different assays revealed the relatively higher cytotoxicity associated with TMPyP than that with TriMPyCOOHP. This behavior could be attributed to the ability of TMPyP to interact with DNA and thereby its ability to exert greater cell damage. Though both TMPyP as well as TriMPyCOOHP exhibited greater cytotoxicity in presence of light as compared to dark, photo-cytotoxic effects were more pronounced in case of former than those observed in case of latter. This observation again could be an indicative of localization of oxidative radicals produced as a result of porphyrin mediated energy transfer, closer to cell DNA owing to TMPyP-DNA interaction. In order to evaluate the comparative *in-vivo* efficacy of both the porphyrin derivatives, they were radiolabeled with ^{68}Ga, a well-known PET radionuclide and the radiolabeled preparations were evaluated in tumor bearing small animal model. The results of bio-distribution studies revealed almost similar uptake of the radiotracers in per gram of tumor mass at the early time point (30 min post-administration) for both ^{68}Ga-TMPyP and ^{68}Ga-TriMPyCOOHP. However, the former exhibited significantly higher retention in the tumor at longer time point (60 min post-administration) compared to the latter. Moreover, the relatively rapid clearance of activity from blood and liver, observed in case of the ^{68}Ga-TMPyP compared to that of ^{68}Ga-TriMPyCOOHP had resulted better tumor to background ratios for the former radiolabeled complex. These observations indicate the important role played by the structure as well as charge of the porphyrin derivatives in controlling their cytotoxicity and tumor affinity.

5. Conclusion

Results of various experiments carried out during present study involving two structurally different porphyrin derivatives viz. TMPyP and TriMPyCOOHP indicate the important role played by the structure as well as charge of the porphyrin derivatives in controlling their pharmacokinetics, cytotoxicity and tumor affinity. These results indicate the importance of preserving all the four cationic centres in the structure of porphyrin derivative as removal of one of them and its replacement with uncharged aliphatic moiety interfered with its DNA binding ability. These observations could be helpful in developing suitable porphyrin derivatives which may have significant role in the management of cancers in the coming days.

Declaration of competing interest

The authors declare that they have no known competing financial interests or personal relationships that could have appeared to influence the work reported in this paper.

Acknowledgement

Bhabha Atomic Research Centre (BARC) is a constituent unit of Department of Atomic Energy, Government of India and all the research activities carried out at the Institute is fully funded by the Government of India.

The authors gratefully acknowledge Dr. P. K. Pujari, Director, Radiochemistry and Isotope Group, BARC for his constant support and encouragement. The authors are thankful to Dr. Ankona Dutta, Ms. Geetanjali Dhotre and the other staff members of the MALDI-TOF facility of Tata Institute of Fundamental Research (TIFR), Mumbai for allowing and helping us in recording the mass spectra of the compounds using MALDI-TOF MS. The authors also express their gratitude to Ms. Mamata Joshi of National NMR Facility, TIFR, Mumbai for providing the facility of recording the NMR spectra reported in the article. The authors also acknowledge Dr. P. A. Hassan, Head Nanotherapeutics and Biosensors Section, Chemistry Division, BARC for providing us the facility of fluorescence imaging. The authors also thank Mr. Umesh Kumar of Radiopharmaceuticals Division, BARC and all the staff members of the Animal House facility, Radiation Biology and Health Sciences Division, BARC for the help provided during the course of the present study.

Appendix A. Supplementary data

Supplementary data to this article can be found online at https://doi.org/10.1016/j.ejmech.2021.113184.

References

[1] A. Policard, Etudes sur les aspects offerts par des tumeurs experimentales examinees a la lumiere de woods, C. R. Soc. Biol. 91 (1924) 14–32.
[2] L.B. Josefsen, R.W. Boyle, Unique diagnostic and therapeutic roles of porphyrins and phthalocyanines in photodynamic therapy, imaging and theranostics, Theranostics 2 (2012) 916–966.
[3] A.H. Kaye, G. Morstyn, M.J. Apuzzo, Photoradiation therapy and its potential in the management of neurological tumors, J. Neurosurg. 69 (1988) 1–14.
[4] P.A. Waghorn, Radiolabeled porphyrins in nuclear medicine, J. Label. Compd. Radiopharm. 57 (2014) 304–309.
[5] Y. Zhou, X. Liang, Z. Dai, Porphyrin-loaded nanoparticles for cancer theranostics, Nanoscale 8 (2017) 12394–12405.
[6] P. Rai, S. Mallidi, X. Zheng, R. Rahmanzadeh, Y. Mir, S. Elrington, A. Khurshid, T. Hasan, Development and applications of photo-triggered theranostic agents, Adv. Drug Deliv. Rev. 62 (2010) 1094–1124.
[7] A.V.C. Simões, S.M.A. Pinto, M.J.F. Calvete, C.M.F. Gomes, N.C. Ferreira, M. Castelo-Brancocd, J. Llope, M.M. Pereira, A.J. Abrunhosa, Synthesis of a new ^{18}F labeled porphyrin for potential application in positron emission tomography: *In vivo* imaging and cellular uptake, RSC Adv. 5 (2015) 99540–99546.

[8] F. Zoller, P.J. Riss, F.P. Montforts, D.K. Kelleher, E. Eppard, F. Rösch, Radiolabelling and preliminary evaluation of ^{68}Ga-tetrapyrrole derivatives as potential tracers for PET, Nucl. Med. Biol. 40 (2013) 280–288.
[9] M. Bhadwal, S. Mittal, T. Das, H.D. Sarma, S. Chakraborty, S. Banerjee, M.R.A. Pillai, Synthesis and biological evaluation of ^{177}Lu-DOTA-porphyrin conjugate: a potential agent for targeted tumor radiotherapy, Q. J. Nucl. Med. Mol. Imaging 58 (2014) 224–233.
[10] M. Bhadwal, T. Das, H.D. Sarma, S. Banerjee, Radiosynthesis and bioevaluation of ^{68}Ga-labeled 5,10,15,20-tetra(4-methylpyridyl)-porphyrin for possible application as a PET radiotracer for tumor imaging, Mol. Imag. Biol. 17 (2015) 111–118.
[11] S. Mittal, M. Bhadwal, T. Das, H.D. Sarma, R. Chakravarty, A. Dash, S. Banerjee, M.R.A. Pillai, Synthesis and biological evaluation of ^{90}Y-labeled DOTA-Porphyrin conjugate: a potent molecule for targeted tumor therapy, Cancer Biother. Radiopharm. 28 (2013) 651–656.
[12] T. Das, S. Chakraborty, H.D. Sarma, S. Banerjee, A novel [^{109}Pd] palladium labeled porphyrin for possible use in targeted radiotherapy, Radiochim. Acta 96 (2012) 427–433.
[13] J.C. Maziere, R. Santus, P. Morliere, J.P. Reyftmann, C. Candide, L. Mora, S. Salmon, C. Maziere, S. Gatt, L. Dubertret, Cellular uptake and photosensitizing properties of anticancer porphyrins in cell membranes and low- and high-density lipoproteins, J. Photochem. Photobiol., B 6 (1990) 61–68.
[14] D. Lazzeri, E.N. Durantini, Synthesis of *meso*-substituted cationic porphyrins as potential photodynamic agents, ARKIVOC 10 (2003) 227–239.
[15] K. Driaf, R. Granet, P. Krausz, M. Kaouadji, F. Thomasson, A.J. Chulia, B. Verneuil, M. Spiro, J.C. Blais, G. Bolbach, Synthesis of glycosylated cationic porphyrins as potential agents in photodynamic therapy, Can. J. Chem. 74 (1996) 1550–1563.
[16] E. Biron, N. Voyer, Synthesis of cationic porphyrin modified amino acids, Chem. Commun. (J. Chem. Soc. Sect. D) 37 (2005) 4652–4654.
[17] A. Garcia-Sampedro, A. Tabero, I. Mahamed, P. Acedo, Multimodal use of the porphyrin TMPyP: from cancer therapy to antimicrobial applications, J. Porphyr. Phthalocyanines 23 (2019) 11–27.
[18] R. Chakravarty, S. Chakraborty, R. Ram, R. Vatsa, P. Bhusari, J. Shukla, B.R. Mittal, A. Dash, Detailed evaluation of different ^{68}Ge/^{68}Ga generators: an attempt toward achieving efficient ^{68}Ga radiopharmacy, J. Label. Compd. Radiopharm. 59 (2016) 87–94.
[19] I. Velikyan, Prospective of ^{68}Ga-radiopharmaceutical development, Theranostics 4 (2014) 47–80.
[20] D. Shetty, Y.S. Lee, J.M. Jeong, ^{68}Ga-Labeled radiopharmaceuticals for positron emission tomography, Nucl. Med. Mol. Imag. 44 (2010) 233–240.
[21] Y. Fazaeli, A.R. Jalilian, M.M. Amini, K. Ardaneh, A. Rahiminejad, F. Bolourinovin, S. Moradkhani, A. Majdabadi, Development of a ^{68}Ga-fluorinated porphyrin complex as a possible PET imaging agent, Nucl. Med. Mol. Imag. 46 (2012) 20–26.
[22] I. Haq, J.O. Trent, B.Z. Chowdhry, T.C. Jenkins, Intercalative G-tetraplex stabilization of telomeric DNA by a cationic porphyrin, J. Am. Chem. Soc. 121 (1999) 1768–1779.
[23] Z. Panagi, A. Beletsi, G. Evangelatos, E. Livaniou, D.S. Ithakissios, K. Avgoustakis, Effect of dose on the biodistribution and pharmacokinetics of PLGA and PLGA-mPEG nanoparticles, Int. J. Pharm. 221 (2001) 143–152.
[24] T. Das, S. Chakraborty, H.D. Sarma, P. Tandon, S. Banerjee, M. Venkatesh, M.R.A. Pillai, ^{170}Tm-EDTMP: a potential cost-effective alternative to $^{89}SrCl_2$ for bone pain palliation, Nucl. Med. Biol. 36 (2009) 561–568.
[25] A.D. Adler, F.R. Longo, J.D. Finarelli, J. Goldmacher, J. Assour, L. Korsakoff, A simplified synthesis for meso-tetraphenylporphine, J. Org. Chem. 32 (1967) 476.
[26] S.Y. Cho, J.H. Han, Y.J. Jang, S.K. Kim, Y.A. Lee, Binding properties of various cationic porphyrins to DNA in the molecular crowding condition induced by poly(ethylene glycol), ACS Omega 5 (2020) 10459–10465.
[27] C.I.V. Ramos, C.M. Barros, A.M. Fernandes, M.G. Santana-Marques, A.J. Ferrer Correia, P.C. Joao, J.P.C. Tomé, M.C.T. Carrilho, M.A.F. Faustino, A.C. Tomé, M.G.P.M.S. Neves, J.A.S. Cavaleiro, Interactions of cationic porphyrins with double-stranded oligodeoxynucleotides: a study by electrospray ionisation mass spectrometry, J. Mass Spectrom. 40 (2005) 1439–1447.
[28] H. Shy, P. Mackin, A.S. Orvieto, D. Gharbharan, G.R. Peterson, N. Bampos, T.D. Hamilton, The two-step mechanochemical synthesis of porphyrins, Faraday Discuss 170 (2014) 59–69.
[29] N. Shirasu, S.O. Nam, M. Kuroki, Tumor-targeted photodynamic therapy, Anticancer Res. 33 (2013) 2823–2832.
[30] K. Hirakawa, Control of Fluorescence and Photosensitized Singlet Oxygen-Generating Activities of Porphyrins by DNA: Fundamentals for Theranostics, 2017, https://doi.org/10.5772/67882. Book Chapter.